The purposes of this study are to quantify pulmonary cysts in CTs of females with both BHDS and LAM and also to identify the independent parameters that enable us to differentiate the two diseases.

2. Materials and methods

2.1. Subjects

This study was approved by the Ethics Committees of Juntendo University (JIRB21-134). This retrospective study included 14 female patients with BHDS and 52 female patients with LAM who had undergone CT scans and pulmonary function tests at our institute between January 2002 and August 2009. The diagnosis of BHDS was obtained with *FLCN* mutation analysis. Some visually evaluated chest CT findings from 9 to 14 patients with BHDS were described previously [10] but are included here because a totally different method was used to assess the pulmonary cysts. LAM was diagnosed from lung biopsies of 42 patients or the biopsy of abdominal and pelvic masses of seven patients. Three patients did not undergo tissue biopsy but had characteristic clinical pictures (recurrent pneumothorax and/or chylous pleural effusion) and CT findings (diffusely scattered thin-walled pulmonary cysts). Three patients were tuberous sclerosis complex (TSC)-associated LAM (TSC-LAM) diagnosed by means of established clinical criteria [15]. All subjects were studied when there was no evidence of pneumothorax, hydrothorax or ascites. The CT scans were performed within a month before or after pulmonary function tests.

2.2. Pulmonary function tests

Pulmonary function tests were performed with an Autospirometer System 9 or Autospirometer System 21 (Minato Medical Science, Osaka, Japan). For all subjects, forced expiratory volume in 1 s (FEV_1) and forced vital capacity (FVC) were measured using the FVC maneuver. Total lung capacity (TLC) and residual volume (RV) were measured using the nitrogen wash-out method. Diffusing capacity for carbon monoxide (TLco) per unit of alveolar volume (VA) was measured using the single-breath technique. VC, FVC, FEV_1, RV/TLC and TLco/VA measurements for each patient were expressed as a percentage of the predicted values (VC% pred, FVC% pred, FEV_1% pred, RV/TLC% pred and TLco/VA% pred) [16].

2.3. Thin-section CT techniques

All patients underwent thin-section CT with an 8-detectors-row CT scanner or 64-detectors-row CT scanner (Aquilion 16 or Aquilion 64; Toshiba Medical, Tokyo, Japan) with a 2-mm slice thickness and scanning parameters of 120 kVp, 150 mAs and a field of view of 32 cm. No contrast media were used. During the scan, the patients held their breath after a deep inspiration in the supine position. Each CT image was composed of a 512×512 matrix of numeric data (CT numbers) in Hounsfield units (HU) using a lung algorithm (FC85). These CT data were transferred to a PowerPC personal computer for quantitative analysis of pulmonary cysts. We confirmed using a phantom of the lungs that there was no difference in data obtained from two CT machines.

2.4. Analysis of pulmonary cysts

Three slices from each patient were analyzed: the upper slice taken 1 cm above the upper margin of the aortic arch; the middle slice taken 1 cm below the carina; and the lower slice taken 1 cm above the top of the diaphragm. We defined lung fields as areas with CT numbers less than −200 HU, whereas the cut-off level between low attenuation areas (LAA) and normal lung density was −960 HU (Fig. 1A and B) [17,18]. Because small discrete continuous LAA (CLA) has been observed in normal lungs, we considered it necessary to distinguish CLA from pulmonary cysts to establish the latters' precise criteria. The smallest diameter of a pulmonary cyst that was visually identifiable on thin-section CT was reported as about 2 mm [12,14,19]. Therefore, we defined the pulmonary cyst as a CLA consisting of 10 or more pixels (Fig. 1C). By this definition, the smallest diameter of pulmonary cyst was about 2.2 mm on CT image if the pulmonary cyst was perfectly round. Next, handmade computer software was used for automatic calculation of the following variables in each slice [17,18]: (1) PC%, percentage of the ratio of pulmonary cysts' areas in each lung field; (2) PCn, the number of pulmonary cysts; (3) PCs, the mean size of pulmonary cysts; and (4) PCc, the mean circularity of pulmonary cysts. Circularity measures the roundness of a pulmonary cyst and was calculated as follows [17]: circularity $= 4\pi$ (area/perimeter^2) and a value near 1.0 indicates nearly circular. Generally, many more small pulmonary cysts are present than large ones. Since the simple average value of circularity for pulmonary cysts is greatly influenced by the values of small ones, it would be inappropriate for the representative value. Therefore, the area-weighted average value of circularity in each slice was calculated as follows. First, the circularity of a pulmonary cyst was multiplied by its own area of each pulmonary cyst. Next, the multiplied value of each pulmonary cyst was totaled. Finally, the total value was divided by the total area of pulmonary cysts, and the resultant number was then defined as PCc. Values of PC%, PCn, PCs and PCc of three lung slices were then averaged for each patient and compared with the two diseases. To compare the distribution of pulmonary cysts in patients with BHDS and LAM, the lung field of each slice was divided vertically into a lateral half and remaining medial region (Fig. 1D). This procedure divided the lung field into six zones (upper-lateral, upper-medial, middle-lateral, middle-medial, lower-lateral and lower-medial). We analyzed the distribution of pulmonary cysts from two aspects: PC% and PCfraction of each lung zone. PCfraction was defined as the ratio (%) of area of pulmonary cysts in each lung zone to the entire area of pulmonary cysts in all six lung zones.

2.5. Statistical analysis

The Chi-square test was used for qualitative variables and unpaired *t*-test for quantitative variables. Univariate (linear) regression analyses were used to evaluate the relationship between any two variables. When there was a significantly different variable between the two diseases, a receiver operating characteristic (ROC) curve was used to examine whether the variables could be used to differentiate the two diseases. A repeated measures two-way analysis of variance (ANOVA) with Tukey's multiple comparison post test was applied to assess the statistical differences of PC% and PCfraction among six lung zones and also between the two diseases. A stepwise discriminant analysis was performed to identify the independent discriminant capability of the parameters with respect to BHDS and LAM while controlling the effect of potential confounders. Wilks' λ was used to assess the significance of the parameters selected. The model validation was performed using jacknife techniques that yield an unbiased estimate of the model classification error. The classification performance of the discriminant function to differentiate the two diseases was also evaluated by using ROC analysis. All statistical analyses were performed using SPSS software (version 16.0, SPSS Inc., Chicago, IL, USA). Data were expressed

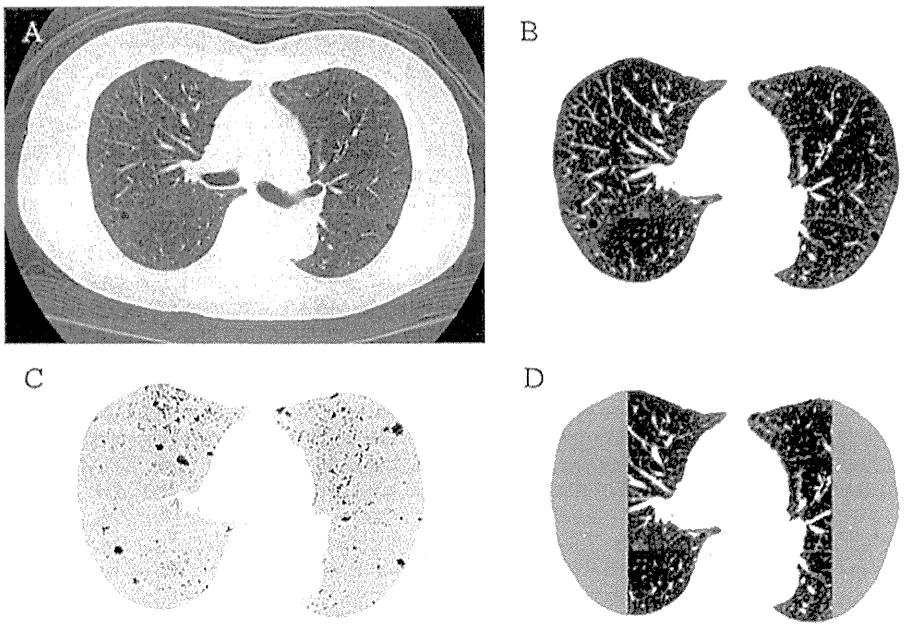

Fig. 1. Representative images of pulmonary cysts classed as CLA in a patient with BHDS. (A) Original CT image at the middle lung slice taken 1 cm below the carina. (B) The lung filed was extracted from the same image as in (A), with the lumen of the trachea and large bronchi excluded. C Individual CLA comprising contiguous LAA regions is shown (black regions). The lung field is identifiable within the image (gray regions). (D) The lung field is divided vertically into the lateral 50% of the lung (gray lateral region) and the remaining medial region.

as means ± SD. A p-value of less than 0.05 was considered significant.

3. Results

3.1. Patient characteristics and pulmonary function

There were significant differences between the patients with BHDS and those with LAM in age, prevalence of family history of pneumothorax within the second degree relatives, FEV_1/FVC and TLCO/VA% pred (Table 1). In contrast, no significant difference was noted between them in the numbers of episodes, surgeries or pleurodesis for pneumothorax.

3.2. Characteristics of pulmonary cysts

Significant differences separated the two groups in all variables representing pulmonary cysts (Table 2). As compared to BHDS, LAM showed increased extent and number, more circular in shape but smaller in size. When we analyzed the extent of pulmonary cysts in each lung zone, LAM showed similar PC% in six lung zones, suggesting homogeneous distribution of cysts throughout the lung field, whereas BHDS patients tended to exhibit an increased PC% toward the medial and lower zones, i.e., the highest percentage in the lower medial zone. The representative CT images of a patient with BHDS and LAM are shown in Fig. 2. Twelve patients with BHDS showed the highest PC% in the lower-medial zone, but only 9 patients with LAM did so ($p < 0.001$, Chi-square test) (Fig. 3A). We defined this characteristic distribution pattern of pulmonary cysts in the 12 BHDS patients as "lower-medial zone predominance of pulmonary cysts". Similarly, when the PCfraction was analyzed, the lower-medial zone predominance of pulmonary cysts remained in the BHDS group (Fig. 3B). The LAM group sustained a lower PCfraction in the two upper lung zones than the remaining four lung zones, presumably reflecting simply the small size of the two upper lung zones.

3.3. Relationships between the features of pulmonary cysts and pulmonary function

When we examined the quantitative variables of pulmonary cysts and pulmonary function in the BHDS and LAM patients (Table 3), only the PCs and FEV_1% pred of BHDS individuals correlated significantly. In contrast, each of four quantitative variables in LAM showed significant correlations: FEV_1/FVC, FEV_1% pred, RV/TLC% pred and TLco/VA% pred. The exception was that between PCn and RV/TLC% pred.

3.4. Discrimination between BHDS and LAM

The final determination was which variables of pulmonary cysts and clinical features are most important for differentiating BHDS from LAM. When we used the presence of family history of pneumothorax within the second degree relatives or the lower-medial zone predominance of pulmonary cysts for the differentiation criteria of BHDS from LAM, the sensitivity/specificity was 0.86/0.83 and 0.43/1.00, respectively. Table 4 presents the results of ROC analyses applied for seven other variables bearing significant differences between the two diseases. Of these seven statistically significant variables, values for TLco/VA% pred and PCn were highest [i.e., area under the ROC curve (Az)]. Finally, we performed a stepwise discriminant analysis by utilizing all variables described above other than age. We did not include age in the discriminant analysis. Because the mean age at a first episode of pneumothorax was almost the same for both diseases, the significant difference of age between the two diseases was presumably from a delayed diagnosis of BHDS. The analysis accepted these four variables: the family history of pneumothorax within the second degree relatives, the lower-medial zone predominance of pulmonary cysts, TLco/VA% pred and PCs in that order (Wilks' $\lambda = 0.310$, $p < 0.001$) (Table 5). With jackknife classification, the diagnostic accuracy was 93.9%; three patients with BHDS and one patient with LAM were incorrectly classified by this model as a member of the other group. Therefore, the point estimates of sensitivity and specificity are 0.79

Table 1
Characteristics and pulmonary function of the BHDS and LAM study population.

	BHDS	LAM
Number of patients	14	52
Age (year)	45.6 ± 14.9 (26–80)	36.4 ± 8.5‡ (20–58)
Smoking history (pack-years)	3.5 ± 8.9 (0–33)	2.0 ± 5.7 (0–33)
Number of patients who experienced PTX	11	36
Age at the first episode of PTX (year)	33.1 ± 11.8 (16–54)	32.0 ± 8.6 (19–53)
Number of PTX (total)	2.6 ± 2.0 (0–6)	2.4 ± 3.6 (0–21)
Left lung	1.4 ± 1.4 (0–4)	1.2 ± 3.0 (0–20)
Right lung	1.1 ± 0.9 (0–3)	1.3 ± 1.7 (0–8)
Number of patients who experienced surgery for PTX	9	29
Number of surgeries for PTX (total)	1.0 ± 1.0 (0–3)	0.8 ± 0.8 (0–2)
Left lung	0.5 ± 0.5 (0–1)	0.3 ± 0.5 (0–2)
Right lung	0.5 ± 0.7 (0–2)	0.5 ± 0.6 (0–2)
Number of patients who experienced pleurodesis for PTX	2	8
Number of pleurodesis for PTX (total)	0.2 ± 0.6 (0–2)	0.3 ± 0.8 (0–4)
Left lung	0.2 ± 0.6 (0–2)	0.2 ± 0.4 (0–2)
Right lung	0	0.2 ± 0.5 (0–2)
Prevalence of family history of PTX within the second degree relatives	6	0‡
Pulmonary function data		
VC% pred (%)	86.7 ± 10.9 (66.0–103.5)	93.8 ± 17.0 (49.2–136.1)
FEV_1/FVC (%)	81.8 ± 7.4 (70.4–93.7)	70.0 ± 18.5† (22.2–99.6)
FEV_1% pred (%)	86.2 ± 13.5 (62.9–104.2)	76.9 ± 24.8 (17.6–111.1)
RV/TLC% pred (%)	107.9 ± 15.3 (86.3–138.2)	114.2 ± 24.5 (68.5–177.3)
TLco/VA% pred (%)	73.6 ± 10.4 (58.4–97.1)	44.6 ± 19.6‡ (9.3–83.3)

TLco, diffusing capacity for carbon monoxide; PTX, pneumothorax; VA, alveolar volume.
Values are expressed as means ± SD where applicable.
Values in parentheses are ranges.
† $p < 0.05$ compared with BHDS by Chi-square test or unpaired t-test.
‡ $p < 0.01$ compared with BHDS by Chi-square test or unpaired t-test.

and 0.98, respectively, for this model. By varying the confidence threshold on the discriminant score, ROC curves were generated and yielded an Az value of 0.989 in differentiating the two diseases.

4. Discussion

This study established significant diagnostic differences between BHDS and LAM and confirmed that the most important

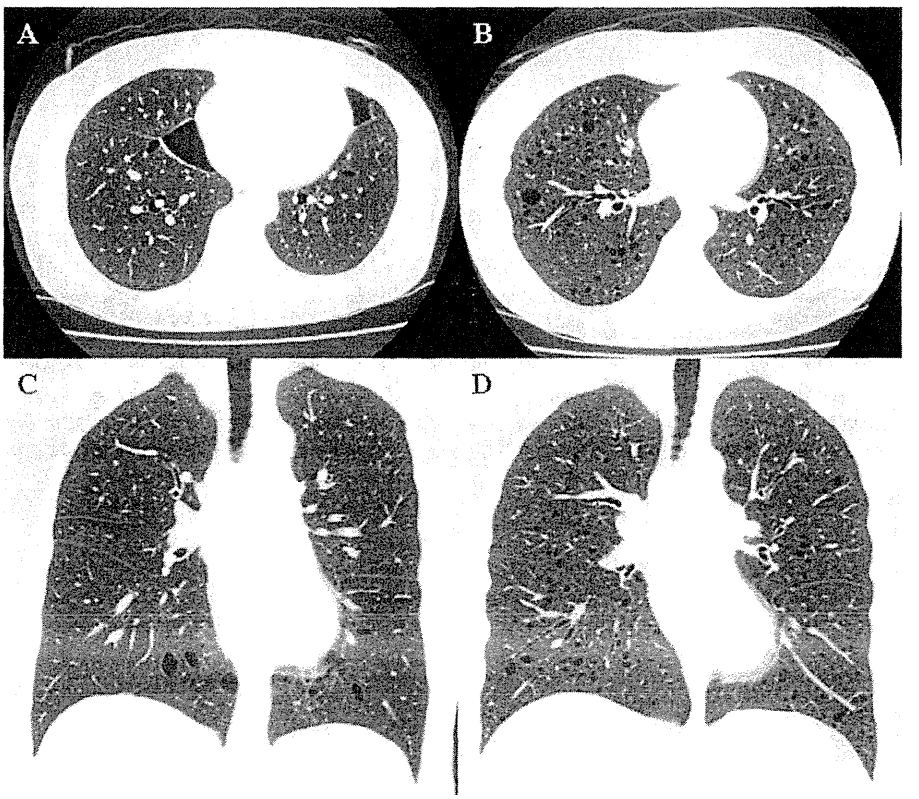

Fig. 2. Representative axial and coronal CT images of patients with BHDS and LAM. Panels (A) and (C): from chest of a 54-year-old female with BHDS. Panels (B) and (D): from chest of a 43-year-old female with LAM.

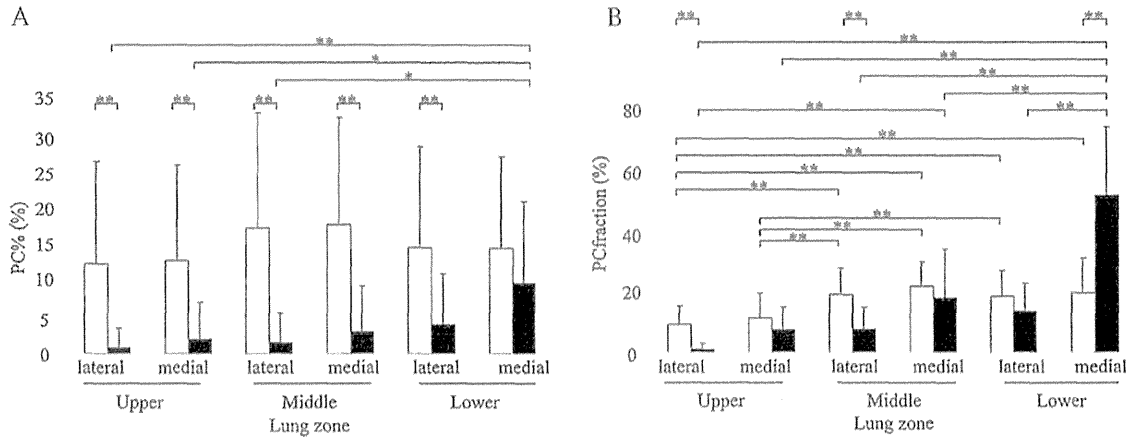

Fig. 3. Comparison of PC% (A) and PCfraction (B) among six lung zones. BHDS, closed bars and LAM, open bars. Values are expressed as mean ± SD. *$p < 0.05$ and **$p < 0.001$ by repeated measures two-way ANOVA with Tukey–Kramer post hoc analysis.

Table 2
Quantitative analyses of pulmonary cysts of BHDS and LAM patients.

	BHDS	LAM
PC% (%)	3.6 ± 5.8 (0.2–22.6)	15.1 ± 13.2‡ (0.1–48.5)
PCn	28.7 ± 66.9 (1.3–259.0)	148.6 ± 102.7‡ (1.3–385.7)
PCs (mm^2)	32.9 ± 21.1 (6.5–80.9)	18.2 ± 11.1† (5.9–57.4)
PCc	0.389 ± 0.114 (0.203–0.571)	0.473 ± 0.128† (0.103–0.724)

Values are expressed as means ± SD.
Values in parenthesis are ranges.
† $p < 0.05$ compared with BHDS by unpaired t-test.
‡ $p < 0.01$ compared with BHDS by unpaired t-test.

variables to investigate for this purpose are the family history of pneumothorax within the second degree relatives, the lower-medial zone predominance of pulmonary cysts, TLco/VA% pred and PCs. Our study is the first report of a quantitative analysis that applies the characteristics of CT-examined pulmonary cysts for the differentiation of two cystic lung diseases with shared clinical features [20,21]. The features of CT images were visually evaluated separately in each of BHDS and LAM by us and other groups [10–14,19]. Our quantitative analyses of pulmonary cysts objectively confirmed that the visual and subjective assessment of pulmonary cysts was appropriate in each disease and furthermore identified which feature of pulmonary cyst contributes to the discrimination of cystic lung diseases with shared clinical features. In the present study, a limited number of TSC-LAM patients may have affected the prevalence of family history of pneumothorax within the second degree relatives. However, it would be rare to find a family history of pneumothorax in TSC due to the following reasons: only female TSC with mild disease can grow to adults, LAM occurs exclusively in women of child-bearing age, and LAM patient may be advised not to become pregnant due to the possible progression of the disease.

To our knowledge, the present study is the first to evaluate pulmonary function in patients with BHDS. In our study, these patients' pulmonary function was almost normal, and only their PC values correlated significantly with FEV_1% pred. This outcome differed considerably from those we observed in patients with LAM and in reports from other groups [19,22–26]. Accordingly, the results of our study suggest that the pathogenesis of cyst formation is quite different in the two diseases. For the mechanism of cyst formation in BHDS, Graham et al. suggested growth failure of the lung [27], whereas Painter et al. attributed the cause to inflammation of the lung [28]. But these hypotheses do not explain the lower-medial zone predominance of pulmonary cysts and almost normal pulmonary function demonstrated by our study; therefore, further investigation is warranted. With respect to LAM, others and we have reported that LAM cells can metastasize by hematogenous [29] or lymphatic dissemination [30], and the protease–antiprotease imbalance plays a role in cyst formation [4]. The diffuse distribution of pulmonary cysts with no zone predominance and the strong correlation between the quantitatively determined variables of pulmonary cysts and functional abnormalities supports the involvement of these mechanisms. In this context, the quantitative and objective assessment of various features of pulmonary cysts has a potential for not only making it possible to discriminate various cystic lung diseases but also to investigate pathogenesis of cystic lung diseases, especially by analyzing serial changes of features of cysts assessed in the present study.

Our study may have several limitations. First, this is a retrospective study, and the number of patients with BHDS included is relatively small. Second, not only pulmonary cysts but also emphy-

Table 3
Correlation coefficients between quantitative variables of pulmonary cysts and pulmonary function in BHDS and LAM patients.

	VC% pred	FEV_1/FVC	FEV_1% pred	RV/TLC% pred	TLco/VA% pred
Patients with BHDS					
PC%	0.046	0.232	0.153	0.007	−0.497
PCn	0.193	0.334	0.357	0.146	−0.465
PCs	−0.265	−0.259	−0.543†	−0.533	0.118
PCc	−0.037	−0.374	−0.085	0.172	0.116
Patients with LAM					
PC%	0.030	−0.840‡	−0.724‡	0.409†	−0.821‡
PCn	0.120	−0.709†	−0.535†	0.263	−0.788‡
PCs	−0.006	−0.686‡	−0.604‡	0.364†	−0.577†
PCc	−0.031	0.542†	0.458†	−0.314†	0.531†

† $p < 0.05$ by linear regression analysis.
‡ $p < 0.01$ by linear regression analysis.

Table 4
Performance for individual variable to differentiate BHDS from LAM.

Variables	Az value	95% CI	*p* value
Age	0.690	0.525–0.855	0.03
FEV_1/FVC	0.687	0.550–0.824	0.04
TLco/VA% pred	0.905	0.834–0.976	<0.01
PC%	0.796	0.677–0.915	<0.01
PCn	0.877	0.761–0.993	<0.01
PCs	0.777	0.627–0.927	<0.01
PCc	0.694	0.545–0.842	0.03

CI, confidence interval.
The area under the ROC curve (Az) is used as an index to evaluate the inherent discriminant capacity of a studied variable in differentiating two diseases. *p*-Values calculated with statistical *Z* tests were used to indicate the significance of the differences between the estimated Az values and an Az value of 0.5.

Table 5
A summary of stepwise discriminant analysis to differentiate BHDS from LAM.

Step	Variables entered	Partial R^2	*F*	*p**
1	Family history of PTX within the second degree relatives	0.266	37.818	<0.001
2	Lower medial zone predominance of pulmonary cysts	0.254	36.077	<0.001
3	TLco/VA% pred	0.200	28.399	<0.001
4	PCs	0.088	12.586	0.001

**p*, significance value.

sema may have been evaluated by the method used here, because each pulmonary cyst in the CT image was defined by the size of CLA. However, Avila et al. reported a good correlation between quantitative measurements of LAA in CT images and abnormalities in pulmonary function in LAM by utilizing the definition of lung fields as areas with CT numbers less than −300 HU and the cut-off level between LAA and normal lung density as −950 HU [24]. The threshold level we used was almost the same as that of Avila et al. Furthermore, the characteristics of pulmonary cysts of BHDS and LAM patients obtained here were consistent with previous reports of others and ours who visually evaluated pulmonary cysts [10]. Therefore, our quantitative analysis of pulmonary cysts is likely to be methodologically adequate, especially for clinical use.

In conclusion, the quantitatively determined characteristics of pulmonary cysts were significantly different between BHDS and LAM. The independent parameters that enabled us to differentiate the two diseases were the family history of pneumothorax within the second degree relatives, characteristics of distribution of pulmonary cysts, diffusing capacity and mean size of pulmonary cysts. The method we used for quantifying the characteristics of pulmonary cysts provides a promising adjunct for the assessment of cystic lung diseases.

Conflict of interest

This study was supported in part by a Grant to the Respiratory Failure Research Group from the Ministry of Health, Labour and Welfare, Japan and the High Technology Research Center Grant from the Ministry of Education, Culture, Sports, Science, and Technology, Japan and the Institute for Environmental and Gender-Specific Medicine, Juntendo University, Graduate School of Medicine.

Acknowledgements

We thank the medical technologists including Mr. Toyoaki Takahashi, Mr. Hideaki Sudo, and Mr. Kazuhiko Doryo of Department of Radiology, Juntendo University Hospital for their assistance in obtaining CT data. This study was supported in part by a Grant to the Respiratory Failure Research Group from the Ministry of Health, Labour and Welfare, Japan and the High Technology Research Center Grant from the Ministry of Education, Culture, Sports, Science, and Technology, Japan and the Institute for Environmental and Gender-Specific Medicine, Juntendo University, Graduate School of Medicine

References

[1] Birt AR, Hogg GR, Dubé WJ. Hereditary multiple fibrofolliculomas with trichodiscomas and acrochordons. Arch Dermatol 1977;113:1674–7.
[2] Nickerson ML, Warren MB, Toro JR, et al. Mutations in a novel gene lead to kidney tumors, lung wall defects, and benign tumors of the hair follicle in patients with the Birt–Hogg–Dubé syndrome. Cancer Cell 2002;2:157–64.
[3] Schmidt LS, Nickerson ML, Warren MB, et al. Germline BHD-mutation spectrum and phenotype analysis of a large cohort of families with Birt–Hogg–Dubé syndrome. Am J Hum Genet 2005;76:1023–33.
[4] McCormack FX. Lymphangioleiomyomatosis: a clinical update. Chest 2008;133:507–16.
[10] Tobino K, Gunji Y, Kurihara M, et al. Characteristics of pulmonary cysts in Birt–Hogg–Dubé syndrome: thin-section CT findings of the chest in 12 patients. Eur J Radiol 2009, doi:10.1016/j.ejrad.2009.09.004.
[11] Sherrier RH, Chiles C, Roggli V, Pulmonary. lymphangioleiomyomatosis: CT findings. Am J Roentgenol 1989;153:937–40.
[12] Lenoir S, Grenier P, Brauner MW, et al. Pulmonary lymphangiomyomatosis and tuberous sclerosis: comparison of radiographic and thin-section CT findings. Radiology 1990;175:329–34.
[13] Kirchner J, Stein A, Viel K, et al. Pulmonary lymphangioleiomyomatosis: high-resolution CT findings. Eur Radiol 1999;9:49–54.
[14] Abbott GF, Rosado-de-Christenson ML, Frazier AA, Franks TJ, Pugatch RD, Galvin JR. From the archives of the AFIP: lymphangioleiomyomatosis: radiologic–pathologic correlation. Radiographics 2005;25:803–28.
[15] Roach ES, Gomez MR, Northrup H. Tuberous sclerosis complex consensus conference: revised clinical diagnostic criteria. J Child Neurol 1998;13:624–8.
[16] Reference values for lung function in the Japanese: recording of normal lung function from 14 institutes in Japan. Jpn J Thoracic Dis 1993;31:421–7.
[17] Sakai N, Mishima M, Nishimura K, Itoh H, Kuno K. An automated method to assess the distribution of low attenuation areas on chest CT scans in chronic pulmonary emphysema patients. Chest 1994;106:1319–25.
[18] Mishima M, Hirai T, Itoh H, et al. Complexity of terminal airspace geometry assessed by lung computed tomography in normal subjects and patients with chronic obstructive pulmonary disease. Proc Natl Acad Sci USA 1999;96:8829–34.
[19] Müller NL, Chiles C, Kullnig P. Pulmonary lymphangiomyomatosis: correlation of CT with radiographic and functional findings. Radiology 1990;175:335–9.
[20] Bonelli FS, Hartman TE, Swensen SJ, Sherrick A. Accuracy of high-resolution CT in diagnosing lung diseases. Am J Roentgenol 1998;170:1507–12.
[21] Koyama M, Johkoh T, Honda O, et al. Chronic cystic lung diseases: diagnostic accuracy of high-resolution CT in 92 patients. Am J Roentgenol 2003;180:827–35.
[22] Aberle DR, Hansell DM, Brown K, Tashkin DP. Lymphangiomyomatosis: CT, chest radiographic, and functional correlations. Radiology 1990;176:381–7.
[23] Crausman RS, Lynch DA, Mortenson RL, et al. Quantitative CT predicts the severity of physiologic dysfunction in patients with lymphangioleiomyomatosis. Chest 1996;109:131–7.
[24] Avila NA, Kelly JA, Dwyer AJ, Johnson DL, Jones EC, Moss J. Lymphangioleiomyomatosis: correlation of qualitative and quantitative thinsection CT with pulmonary function tests and assessment of dependence on pleurodesis. Radiology 2002;223:189–97.
[25] Paciocco G, Uslenghi E, Bianchi A, et al. Diffuse cystic lung diseases: correlation between radiologic and functional status. Chest 2004;125:135–42.
[26] Schmithorst VJ, Altes TA, Young LR, et al. Automated algorithm for quantifying the extent of cystic change on volumetric chest CT: initial results in lymphangioleiomyomatosis. Am J Roentgenol 2009;192:1037–44.
[27] Graham RB, Nolasco M, Peterlin B, Garcia CK. Nonsense mutations in folliculin presenting as isolated familial spontaneous pneumothorax in adults. Am J Respir Crit Care Med 2005;172:39–44.
[28] Painter JN, Tapanainen H, Somer M, Tukiainen P, Aittomäki K. A 4-bp deletion in the Birt–Hogg–Dube gene (FLCN) causes dominantly inherited spontaneous pneumothorax. Am J Hum Genet 2005;76:522–7.
[29] Crooks DM, Pacheco-Rodriguez G, DeCastro RM, et al. Molecular and genetic analysis of disseminated neoplastic cells in lymphangioleiomyomatosis. Proc Natl Acad Sci USA 2004;101:17462–7.
[30] Kumasaka T, Seyama K, Mitani K, et al. Lymphangiogenesis-mediated shedding of LAM cell clusters as a mechanism for dissemination in lymphangioleiomyomatosis. Am J Surg Pathol 2005;29:1356–66.

Further reading

[5] Johnson SR. Lymphangioleiomyomatosis. Eur Respir J 2006;27:1056–65.

[6] Moss J, Avila NA, Barnes PM, et al. Prevalence and clinical characteristics of lymphangioleiomyomatosis (LAM) in patients with tuberous sclerosis complex. Am J Respir Crit Care Med 2001;164:669–71.
[7] Franz DN, Brody A, Meyer C, et al. Mutational and radiographic analysis of pulmonary disease consistent with lymphangioleiomyomatosis and micronodular pneumocyte hyperplasia in women with tuberous sclerosis. Am J Respir Crit Care Med 2001;164:661–8.
[8] Costello LC, Hartman TE, Ryu JH. High frequency of pulmonary lymphangioleiomyomatosis in women with tuberous sclerosis complex. Mayo Clin Proc 2000;75:591–4.
[9] Crino PB, Nathanson KL, Henske EP. The tuberous sclerosis complex. N Engl J Med 2006;355:1345–56.

Human Pathology (2012) 43, 1777–1784

ELSEVIER

Human PATHOLOGY

www.elsevier.com/locate/humpath

Case study

Uterine angiosarcoma associated with lymphangioleiomyomatosis in a patient with tuberous sclerosis complex: an autopsy case report with immunohistochemical and genetic analysis☆,☆☆

Takuo Hayashi MD, PhD[a,b,*], Kengo Koike MD, PhD[b,c], Toshio Kumasaka MD, PhD[b,d], Tsuyoshi Saito MD, PhD[a], Keiko Mitani MT, CT, (IAC)[a,b], Yasuhisa Terao MD, PhD[e], Daiki Ogishima MD, PhD[f], Takashi Yao MD, PhD[a], Satoru Takeda MD, PhD[e], Kazuhisa Takahashi MD, PhD[c], Kuniaki Seyama MD, PhD[b,c]

[a]*Department of Human Pathology, Juntendo University School of Medicine, 2-1-1, Hongo, Bunkyo-ku, Tokyo 113-8421, Japan*
[b]*The Study Group of Pneumothorax and Cystic Lung Diseases, Japan*
[c]*Department of Respiratory Medicine, Juntendo University School of Medicine, 2-1-1, Hongo, Bunkyo-ku, Tokyo 113-8421, Japan*
[d]*Department of Pathology, Japanese Red Cross Medical Center, 4-1-22, Hiroo, Shibuya-ku, Tokyo, Japan*
[e]*Department of Gynecology and Obstetrics, Juntendo University School of Medicine, Tokyo 150-8935, Japan*
[f]*Department of Gynecology and Obstetrics, Juntendo University Nerima Hospital, 3-1-10, Takanodai, Nerima-ku, Tokyo 177-8521, Japan*

Received 10 January 2012; revised 9 March 2012; accepted 9 March 2012

Keywords:
Lymphangioleiomyomatosis;
Angiosarcoma;
Tuberous sclerosis complex

Summary A 41-year-old woman carrying a germline tuberous sclerosis complex 2 (*TSC2*) mutation, whose regular medical follow-up for tuberous sclerosis complex and tuberous sclerosis complex–associated lymphangioleiomyomatosis had continued for 2 years, had uterine angiosarcoma concomitant with uterine lymphangioleiomyomatosis. Immunohistochemically, the uterine angiosarcoma cells showed an extremely skewed lymphatic differentiation; they were diffusely immunopositive for CD31 but negative for other vascular endothelial markers including factor VIII and CD34 yet strongly immunopositive for lymphatic endothelial markers including D2-40 and Prox-1. Loss of heterozygosity analysis demonstrated that not only lymphangioleiomyomatosis and renal angiomyolipoma but also the uterine angiosarcoma had loss of heterozygosity on *TSC2*. Furthermore, direct sequencing revealed a *TP53* mutation in the uterine angiosarcoma. Collectively, the findings suggest that combined dysfunction of the p53 and *TSC2* tumor suppressor proteins may contribute to the development of uterine angiosarcoma in this rare clinical setting.

☆ Disclosures: The authors have no conflicts of interest to disclose.

☆☆ This study was supported by a Grant-in-Aid for Scientific Research No. 19590406 (Dr Kumasaka), No. 23590434 (Dr Saito), and No. 18390243 (Dr Seyama); in part by the High Technology Research Center Grant from the Ministry of Education, Culture, Sports, Science, and Technology, Japan, and in part by a grant to the Respiratory Failure Research Group from the Ministry of Health, Labor, and Welfare, Japan.

* Corresponding author. Department of Human Pathology, Juntendo University School of Medicine, 2-1-1, Hongo, Bunkyo-Ku, Tokyo 113-8421, Japan.
E-mail address: tkhyz@juntendo.ac.jp (T. Hayashi).

0046-8177/$ – see front matter
doi:10.1016/j.humpath.2012.03.020

1. Introduction

Angiosarcomas usually arise in skin and soft tissue as de novo or against a background of long-standing lymphedema, most commonly after a mastectomy. Other anatomical sites where angiosarcomas develop include breast, liver, bone, spleen, heart and great vessels, orbit, pharynx, and oral cavity. Radiation therapy and chemotherapy have been proposed as risk factors for angiosarcomas, and *TP53* mutations are identified in angiosarcomas of the liver [1]. In contrast, uterine sarcomas other than leiomyosarcomas and endometrial stromal sarcomas are uncommon. In particular, the uterine angiosarcoma is very rare, and fewer than 20 well-documented cases have been reported. Most patients were postmenopausal and generally presented with heavy uterine bleeding, weight loss, and pelvic mass. Uterine angiosarcomas are usually highly aggressive and extend beyond the uterus, sometimes recurring within weeks to months of initial diagnosis. Angiosarcoma cells are immunopositive for endothelial markers including CD31, CD34, and factor VIII, but the contributory molecular alterations are unknown. Here we present data from an autopsy of a patient with tuberous sclerosis complex (TSC)–associated lymphangioleiomyomatosis (LAM) complicated by a uterine angiosarcoma. In this rare clinical setting, we performed immunohistochemical and genetic analyses to elucidate possible mechanisms by which a uterine angiosarcoma developed during the course of TSC-associated LAM.

2. Case report

This 39-year-old woman was admitted to a local hospital because of severe lower abdominal pain and vaginal discharge. She had a family history of TSC because her father had facial angiofibromas and underwent a nephrectomy due to renal angiomyolipomas. Her facial angiofibromas had been recorded since age 10 years, and a right pneumothorax occurred when she was 33 years old. Thereafter, she gradually experienced exertional dyspnea. Thorough examinations using computed tomography and magnetic resonance imaging resulted in a diagnosis of TSC with LAM as well as renal and hepatic angiomyolipomas, but no abnormalities appeared in her abdomen or pelvic cavity. The diagnosis of LAM was established from pathologic analysis of a transbronchial lung biopsy. Monthly subcutaneous injections of gonadotropin-releasing hormone analogue (leuprorelin acetate 1.88 mg) followed in the hope of stabilizing the LAM.

At the age of 41 years, she experienced abdominal distention, lower abdominal pain, and uterine bleeding. A computed tomographic scan of her lower abdomen and pelvic cavity revealed an enlarged uterus and swelling of the retroperitoneal lymph nodes from her lower abdomen to the pelvic cavity. An endometrial biopsy resulted in a diagnosis of high-grade sarcoma. Her uterus and bilateral adnexa were subsequently resected. Histopathologic and immunohistochemical examinations of those resected specimens revealed uterine angiosarcoma and LAM. Neither chemotherapy nor radiation therapy was performed after the surgery. The angiosarcoma recurred locally and then metastasized to her liver and lungs 6 months after surgery, followed by her death. An autopsy was performed with a written informed consent.

3. Materials and methods

3.1. Histopathologic and immunohistochemical examination

All tissues were fixed in 10% buffered formalin and embedded in paraffin after routine processing, sectioning, and staining with hematoxylin and eosin (H&E). Immunostaining was performed with antibodies directed to the following: vimentin (dilution 1:500; Dako Cytomation, Carpinteria, CA), CD31 (dilution 1:100; Dako Cytomation), CD34 (dilution 1:200; Novocastra Laboratories Ltd, New Castle, UK), factor VIII (dilution 1:300; Dako Cytomation), D2-40 (dilution 1:200; Dako Cytomation), Prox-1 (dilution 1:750; AngioBio, Del Mar, CA), VEGF-A (dilution 1:200; R&D Co Ltd, Minneapolis, MN), VEGF-C (dilution 1:200; R&D Co Ltd), VEGF-D (dilution 1:200; R&D Co Ltd), VEGFR-3 (dilution 1:50; R&D Co Ltd), c-kit (dilution 1:200; Dako Cytomation), p53 (dilution 1:200; Dako Cytomation), α smooth muscle actin (αSMA) (dilution 1:200; Dako Cytomation), HMB45 (dilution 1:50; Dako Cytomation), estrogen receptor (ER) (dilution 1:50; Novocastra Laboratories Ltd), and progesterone receptor (PgR) (dilution 1:50; Novocastra Laboratories Ltd). An EnVision kit (Dako Cytomation) was used for the immunostaining of vimentin, CD31, CD34, factor VIII, D2-40, Prox-1, VEGF-A, p53, c-kit, αSMA, HMB45, ER, and PgR to detect binding of the first antibodies according to the manufacturer's instructions, and 3,3′-diaminobenzidine tetrahydrochloride was used as the chromogen. For immunostaining of VEGF-C, VEGF-D, and VEGFR-3, biotinylated antigoat rabbit antibody (Dako Cytomation) and alkali phosphatase-conjugated streptavidin (Dako Cytomation) were used to detect antibody binding. Fast red was used as the chromogen.

3.2. Loss of heterozygosity analysis of the *TSC1* and *TSC2* gene-associated regions

The angiosarcoma, LAM, and angiomyolipoma were analyzed for loss of heterozygosity (LOH) on chromosome 9q (including the *TSC1* gene-associated region) and 16p (including the *TSC2* gene-associated region). Genomic DNA was extracted from the following tissues: angiosarcoma in the uterus, LAM in the retroperitoneal lymph node, and angiomyolipoma in the kidney. All tissues were fixed in 10%

buffered formalin and embedded in paraffin after routine processing. Eight-micrometer-thick specimens were sectioned from each block for microdissection. To eliminate contamination during microdissection, inflammatory cells in at least 2 mm^2 area of lesions were removed by laser capture microdissection (Leica Microsystems GmbH, Wetzlar, Germany). Then, tumor cells remaining after laser capture microdissection, that is, angiosarcoma, LAM, or angiomyolipoma, were scraped out with a 27-gauge needle. Normal tissue samples from sites including the uterus and kidney were microdissected as normal controls. DNA from the scraped tissues was extracted with 25 μL extraction buffer consisting of 50 mM Tris-HCl (pH8.0), 1 mM EDTA, and 0.5% Tween 20 and 1/50 volume of proteinase K solution (10 mg/mL). We used the following 12 microsatellite markers: *D9S149*, *D9S2126*, *D9S1830*, *D9S1199*, *S9S1198*, *D9S150*, *D16S521*, *D16S525*, *Kg8*, *D16S291*, *D16S663*, and *D16S283*. Polymerase chain reaction (PCR) was performed as we previously described [2]. LOH analysis was carried out using an Applied Biosystems 3130/3130xl Genetic Analyzer and a Gene Mapper 4.0 (both from Applied Biosystems, Foster City, CA). To confirm reproducibility, all lesions were examined at least twice. A reduction in signal intensity over 50% was defined as LOH.

3.3. Mutation analysis of the TSC genes and TP53 gene

Genomic DNA isolated from peripheral blood leukocytes was used to identify a germline mutation of the *TSC* genes according to the method described previously [3]. Briefly, each exon of the *TSC1* and *TSC2* gene was separately amplified and then screened by single-strand conformational polymorphism analysis. When mobility shift was detected, sequencing of the exon of concern was performed using an automated sequencer (ABI Prism BigDye Terminator v1.1 Cycle Sequencing kit and ABI 3130 Genetic Analyzer; both from Applied Biosystems). Cloning of the PCR product was performed using TA cloning kit (Invitrogen, Carlsbad, CA). Mutations of the *TP53* gene were examined using DNA extracted from angiosarcoma from exons 5 to 9 by direct sequencing. The primer sequences used in this study have been previously described [4].

4. Results

4.1. Genetic confirmation of the diagnosis of TSC

Mutation analysis identified a germline mutation on exon 36 of the *TSC2* gene, an in-frame deletion of isoleucine at the amino acid 1614 position (Fig. 1), thereby confirming the diagnosis of TSC. This mutation is reported to be pathogenic and listed in the LOVD Tuberous sclerosis database (http://chromium.liacs.nl/LOVD2/TSC/home.php?select_db=TSC2).

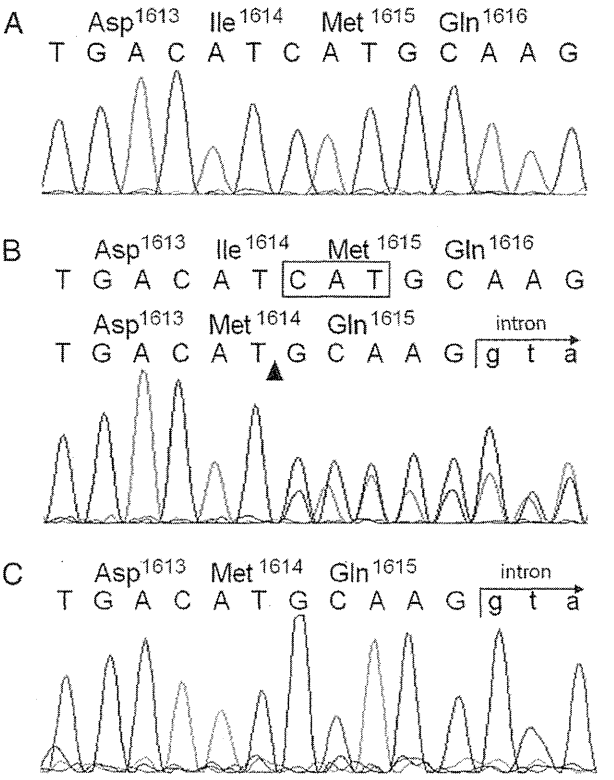

Fig. 1 A germline mutation was demonstrated in exon 36 of the *TSC2* gene. Sequencing of exon 36 of the *TSC2* gene using genomic DNA revealed the wild-type sequence in a normal control (A) but superimposed nucleotide chromatograms near the end of exon 36 in the patient (B). C, Cloning of the patient's PCR product identified clones carrying the wild-type sequence and those carrying a deletion of 3 nucleotides (c.4842_4844del-CAT), resulting in an in-frame deletion of isoleucine at the amino acid 1614 position (C).

4.2. Pathologic findings in the uterus and adnexa

On macroscopic examination, enlargement of the uterus was established from a measurement of 14 × 12 × 9 cm and weight of 660 g. The entire uterus was involved by hemorrhagic and necrotic areas alternated with scattered white solid masses. Microscopically, areas of solid growth with hemorrhage or necrosis constituted a major component of the uterine lesions and were composed of spindle or epithelioid-shaped tumor cells with nuclear pleomorphism and prominent mitotic activity. Tumor cells infiltrated into the uterine myometrium with irregular margins and formed a rudimentary lumen focally. Furthermore, small numbers of tumor cells showed rhabdoid features. Immunohistochemically, tumor cells were diffusely positive for vimentin, CD31, Prox-1, p53, VEGF-A, VEGF-C, and VEGF-D, focally positive for D2-40 and c-kit. On the other hand, these cells were negative for CD34, factor VIII, αSMA, HMB45, ER, and PgR (Fig. 2). Based on the histologic and immunohistochemical findings, we made a diagnosis of

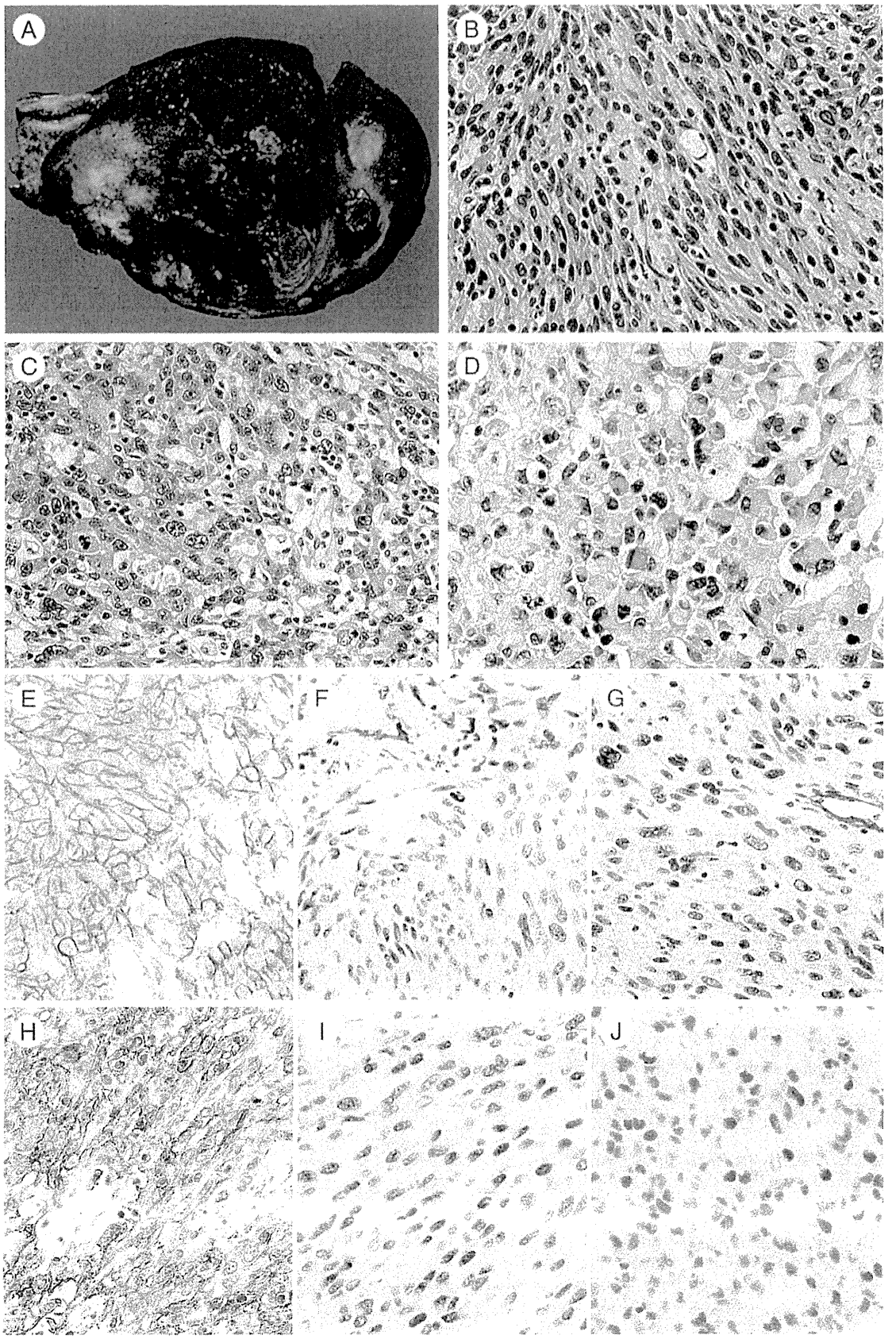
A
B
C
D
E
F
G
H
I
J

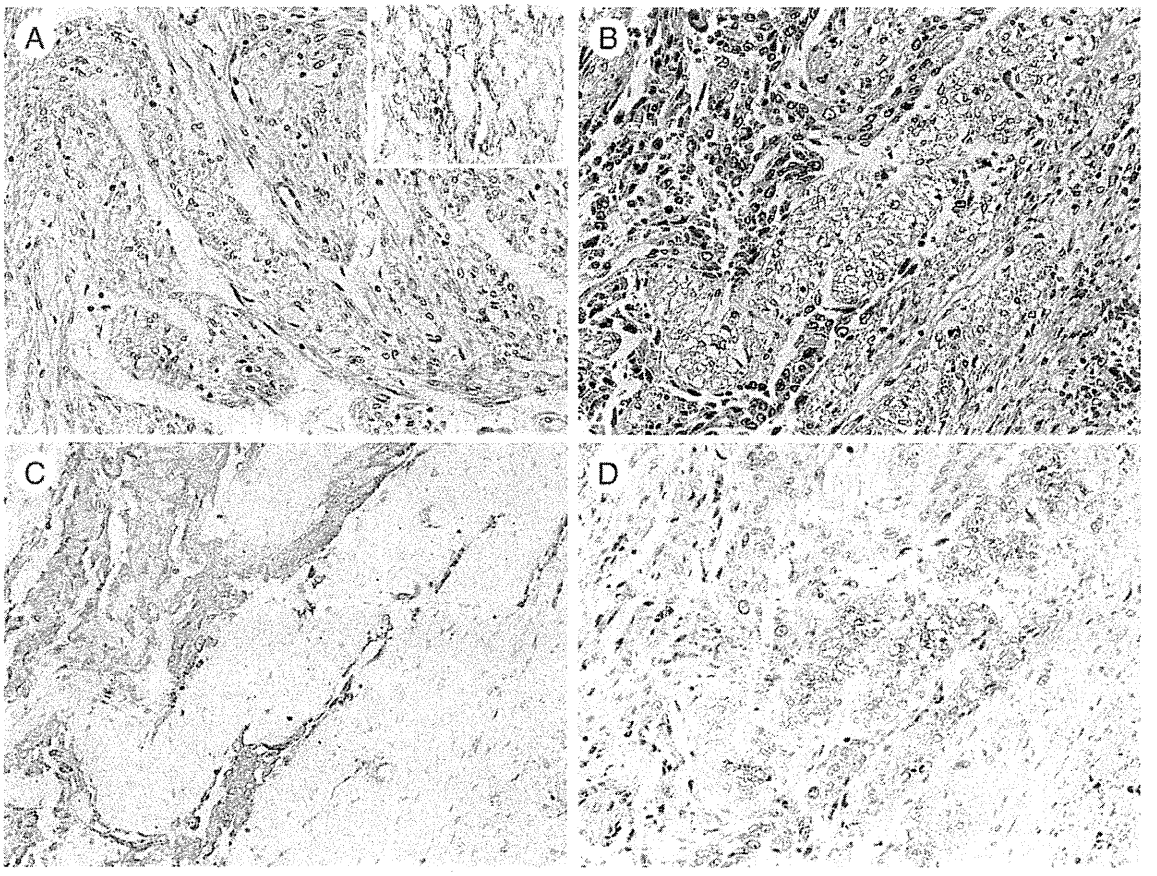

Fig. 3 LAM and angiosarcoma in the uterus. A, LAM cells were arranged in fascicles around slit-like spaces. The inset in A shows immunoreactivity for HMB45. B, Uterine LAM and angiosarcoma were intermixed, and angiosarcoma cells (left) proliferated in slit-like spaces within LAM lesions in some areas. (A-B, H&E stain). C, Immunohistochemically, LAM cells were negative for VEGFR-3, whereas slit-like spaces were covered by VEGFR-3–positive lymphatic endothelial cells. In addition, angiosarcoma cells, which proliferated in LAM-associated lymphatic vessels, were strongly immunoreactive for VEGFR-3. D, On the other hand, LAM cells were strongly positive for VEGF-D, but angiosarcoma cells were only weakly positive for VEGF-D. (Original magnification: A-D, ×100.)

uterine angiosarcoma. In addition, the uterus had a mixed population of small to medium-sized spindle or epithelioid-shaped LAM cells in a tongue-like growth pattern, as we previously described [5]. Immunohistochemically, LAM cells were positive for vimentin, αSMA, ER, PgR, and HMB45, VEGF-C, and VEGF-D, whereas they were negative for CD31, CD34, factor VIII, VEGF-A, D2-40, Prox-1, c-kit, and p53. Slit-like spaces within LAM lesions were covered by flattened cells positive for D2-40 and VEGFR-3, that is, lymphatic endothelial cells. Cells of LAM and angiosarcoma were intermixed in the myometrium, and those of angiosarcoma proliferated within intra-LAM lesional lymphatic vessels in some areas. Furthermore, angiosarcoma cells proliferating in lymphatic vessels within LAM lesions were strongly immunoreactive for VEGFR-3, although angiosarcoma cells at other sites were weakly to moderately immunopositive for VEGFR-3 (Fig. 3). The right and left ovaries measured 2.6 × 1.9 cm and 4.3 × 1.3 cm, respectively. Neither ovary showed any metastatic foci of angiosarcoma, but LAM lesions were detected in the ovaries and broad ligament microscopically.

Fig. 2 Pathologic findings of the uterine angiosarcoma. A, Macroscopically, the uterus was enlarged with a marked hemorrhagic cut surface. B, Most tumor cells were spindle-shaped and displayed a high nuclear/cytoplasmic ratio. C, Some areas also contained epithelioid-shaped cells with prominent nuclei, and tumor cells focally formed a rudimentary lumen. D, Small numbers of tumor cells showed rhabdoid features. (B-D, H&E stain). Immunohistochemical analysis revealed diffuse and strong positivity for CD31 (E) but negative for factor VIII (F) and CD34 (G) yet strongly immunopositive for lymphatic endothelial markers including D2-40 (H) and Prox-1 (I). J, Tumor cells were diffusely positive for p53. (Original magnification: B-D, ×180; E-J, ×160.)

4.3. Autopsy findings

At autopsy, bloody ascites (150 mL) and bloody pleural effusions (left, 200 mL; right, 1500 mL) were present. In the pelvic mass (17 × 14 cm), local recurrence, peritoneal dissemination, and metastatic lesions of angiosarcoma in lymph nodes were detectable. The angiosarcoma also metastasized to mediastinal lymph nodes, both lungs, liver, both kidneys, and thoracic vertebra. In addition, the following lesions associated with TSC were identified: LAM in both lungs and lymph nodes including mediastinal, retroperitoneal, and pelvic lymph nodes; angiomyolipomas of both kidneys and liver; multifocal micronodular pneumocyte hyperplasia of both lungs; and tubers of the cerebrum.

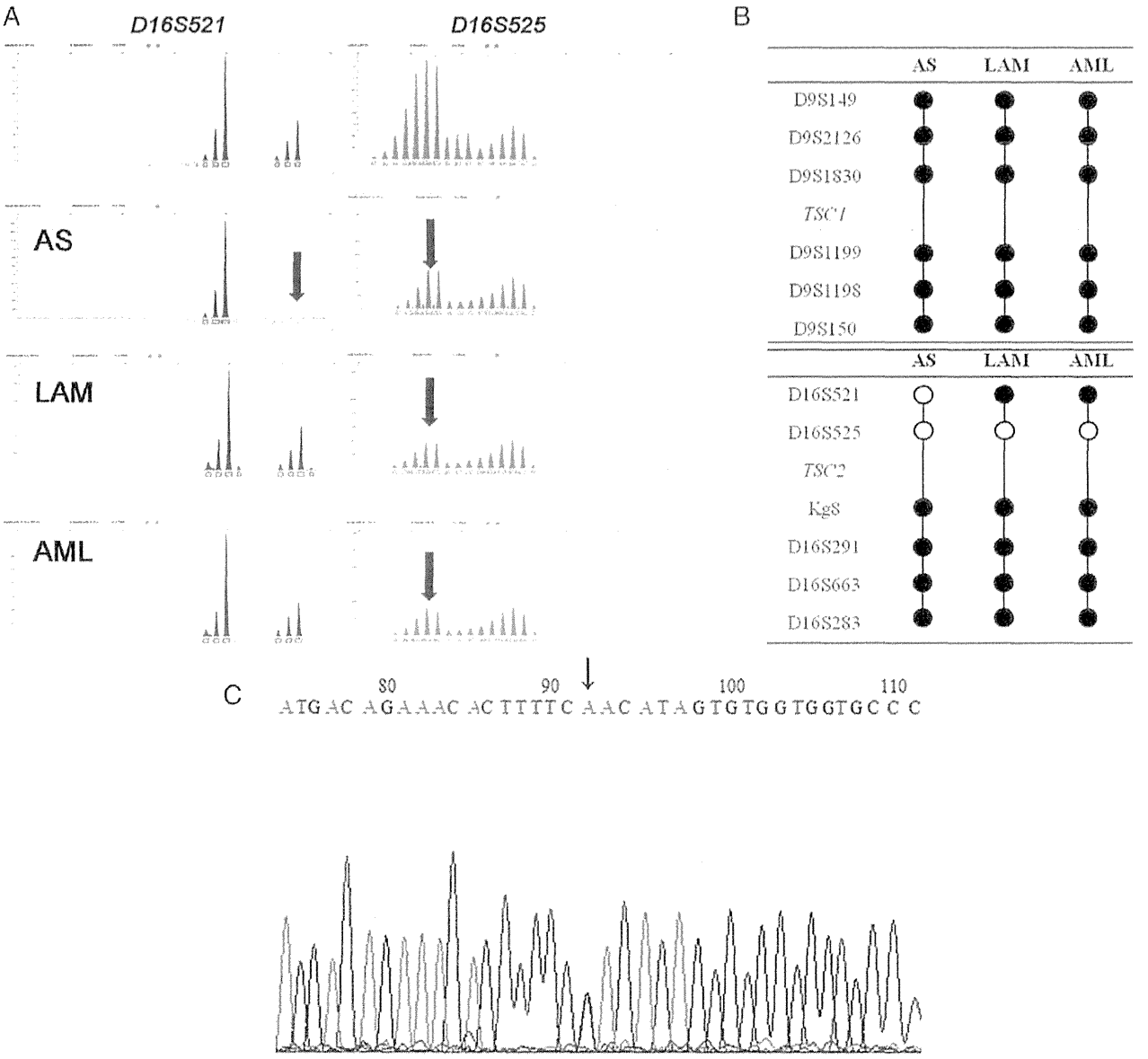

Fig. 4 Genetic analysis. A, Representative results of LOH analysis. Only angiosarcoma cells (AS) microdissected from the uterus showed LOH at *D16S521* in which the allele of larger size disappeared completely; both alleles at *D16S521* were retained in LAM cells and angiomyolipoma cells (AML). In contrast, all lesions examined showed LOH at *D16S525* in which the allele of a smaller size was reduced by more than 50%. B, LOH analysis for *TSC1*- and *TSC2*-associated loci in AS, LAM, and AML is summarized. Open circles indicate the identification of LOH, and closed circles indicate the absence of LOH. C, Mutation of the *TP53* gene in angiosarcoma cells. Direct sequencing of DNA isolated from microdissected angiosarcoma cells revealed a substitution of A to G in codon 213, resulting in an amino acid change from arginine (CAA) to glutamine (CGA).

4.4. LOH analysis on the TSC1 gene- and TSC2 gene-associated regions

LAM, angiomyolipoma, and angiosarcoma showed an identical pattern of LOH at *D16S525*. However, only the angiosarcoma had LOH at *D16S521*, which was located next to *D16S525*. None of the lesions manifested LOH on chromosome 9q (Fig. 4A, B).

4.5. Mutation analysis of the TP53 gene

The uterine angiosarcoma harbored a *TP53* point mutation in exon 6. Direct sequencing showed a substitution of CAA for CGA at codon 213 resulting in an amino acid change from arginine to glutamine (Fig. 4C).

5. Discussion

We describe here, for the first time, a patient with TSC who had uterine angiosarcoma and LAM. To the best of our knowledge, uterine angiosarcoma concomitant with LAM has not been reported previously. Although this patient resembled others in terms of clinical symptoms and outcomes, this angiosarcoma displayed greater lymphatic differentiation than other uterine angiosarcoma reported in the literature because these tumor cells were immunopositive for the lymphatic endothelial markers D2-40 and Prox-1 but completely negative for the vascular endothelial markers CD34 and factor VIII. Although lymphatic differentiation is not uncommon in angiosarcomas and some subsets of tumor cells show greater lymphatic differentiation than others [6], most of the angiosarcoma cells in our patient were unique in their immunopositivity for Prox-1, which is a master regulator of the lymphatic vasculature phenotype [7]. Conceivably, this angiosarcoma underwent extremely skewed differentiation into a lymphatic phenotype, possibly related to the clinical setting, that is, TSC-associated LAM, a disease known for abundant lymphatic vessels induced by LAM-associated lymphangiogenesis [8].

Autopsy findings confirmed the multisystemic and multifocal nature of TSC, and mutation analysis of the *TSC2* gene supported the clinical diagnosis. We also analyzed both LAM and renal angiomyolipoma for second-hit mutations and found LOH in the *TSC2* region, indicating inactivation of the second allele in both lesions. These results confirmed current understanding that hamartomatous proliferation in TSC is caused by constitutive activation of the mammalian target of rapamycin signaling pathway dysregulated by a functional loss of the *TSC* genes. Furthermore, LAM and angiomyolipoma of the kidney had an identical LOH pattern similar to that in another study [9], suggesting that LAM and angiomyolipoma may have a common genetic origin.

Of interest, and unique to this case, was the uterine angiosarcoma's LOH in the *TSC2* region, suggesting that Knudson's 2-hit tumor suppressor gene theory may have applied to the development of angiosarcoma in our patient as well as her LAM and renal angiomyolipoma. The cause of angiosarcoma in this infrequent clinical setting remains largely speculative, but one explanation may be as follows. First, angiosarcoma cells might have originated from lymphatic endothelial cells within LAM lesions. Like Stewart-Treves syndrome, in which long-standing postmastectomy lymphedema and regional immune deficiency are postulated to play a role in the complication of angiosarcoma, uterine LAM and LAM-associated lymphangiogenesis might have resulted in the intrauterine and intrapelvic lymphostasis and subsequent occurrence of angiosarcoma in our present patient. We demonstrated that LAM cells carrying *TSC2* LOH; however, we could not examine whether intra-LAM lesional lymphatic endothelial cells carried the same *TSC2* LOH because of the technical difficulty of microdissecting such a small number of lymphatic endothelial cells. However, considering the clinical background of patients with TSC who carry a germline *TSC2* mutation, we conjectured, first, that some lymphatic endothelial cells might have undergone successive genetic alterations of *TSC2* and *TP53* eventually leading to the malignant transformation that produced angiosarcoma cells during the proliferation of lymphatic endothelial cells driven by LAM-associated lymphangiogenesis. Second, angiosarcoma cells might have been derived from LAM cells as a malignant progression. Liang el al postulated that malignant uterine perivascular epithelioid cell tumor (PEComa) resulted from the malignant transformation of LAM cells because both were immunoreactive for HMB45 and αSMA [10]. However, our patient's angiosarcoma cells expressed neither αSMA nor HMB45, and her immunoprofile of uterine angiosarcoma clearly differed from that of uterine LAM. Finally, we cannot exclude the possibility that the uterine angiosarcoma was not associated with LAM but might have simply occurred de novo. That is, the clinical setting of TSC typically includes the development of tumors in multiple systems and organs. However, the angiosarcoma has not been recognized so far as a tumor that commonly complicates the condition of patients with the TSC.

Acknowledgment

We thank Phyllis Minick for excellent assistance in the review of English.

References

[1] Weihrauch M, Markwarth A, Lehnert G, et al. Abnormalities of the ARF-p53 pathway in primary angiosarcomas of the liver. HUM PATHOL 2002;33:884-92.

[2] Hayashi T, Kumasaka T, Mitani K, et al. Loss of heterozygosity on tuberous sclerosis complex genes in multifocal micronodular pneumocyte hyperplasia. Mod Pathol 2010;23:1251-60.
[3] Sato T, Seyama K, Fujii H, et al. Mutation analysis of the TSC1 and TSC2 genes in Japanese patients with pulmonary lymphangioleiomyomatosis. J Hum Genet 2002;47:20-8.
[4] Kawaguchi K, Oda Y, Nakanishi K, et al. Malignant transformation of renal angiomyolipoma: a case report. Am J Surg Pathol 2002;26: 523-9.
[5] Hayashi T, Kumasaka T, Mitani K, et al. Prevalence of uterine and adnexal involvement in pulmonary lymphangioleiomyomatosis: a clinicopathologic study of 10 patients. Am J Surg Pathol 2011;35: 1776-85.
[6] Mankey CC, McHugh JB, Thomas DG, Lucas DR. Can lymphangiosarcoma be resurrected? A clinicopathological and immunohistochemical study of lymphatic differentiation in 49 angiosarcomas. Histopathology 2010;56:364-71.
[7] Hong YK, Detmar M. Prox1, master regulator of the lymphatic vasculature phenotype. Cell Tissue Res 2003;314:85-92.
[8] Seyama K, Kumasaka T, Kurihara M, et al. Lymphangioleiomyomatosis: a disease involving the lymphatic system. Lymphat Res Biol 2010;8:21-31.
[9] Yu J, Astrinidis A, Henske EP. Chromosome 16 loss of heterozygosity in tuberous sclerosis and sporadic lymphangiomyomatosis. Am J Respir Crit Care Med 2001;164:1537-40.
[10] Liang SX, Pearl M, Liu J, et al. "Malignant" uterine perivascular epithelioid cell tumor, pelvic lymph node lymphangioleiomyomatosis, and gynecological pecomatosis in a patient with tuberous sclerosis: a case report and review of the literature. Int J Gynecol Pathol 2008;27: 86-90.

European Journal of Radiology 81 (2012) 3925–3930

Contents lists available at SciVerse ScienceDirect

European Journal of Radiology

journal homepage: www.elsevier.com/locate/ejrad

Quantitative CT analysis of small pulmonary vessels in lymphangioleiomyomatosis

Katsutoshi Ando[a,e,*], Kazunori Tobino[b,e], Masatoshi Kurihara[c,e], Hideyuki Kataoka[c,e], Tokuhide Doi[d], Yoshito Hoshika[a,e], Kazuhisa Takahashi[a], Kuniaki Seyama[a,e]

[a] Department of Internal Medicine, Division of Respiratory Medicine, Juntendo University Graduate School of Medicine, 2-1-1 Hongo, Bunkyo-Ku, Tokyo 113-8421, Japan
[b] Department of Respiratory Medicine, Iizuka Hospital, 3-83 Yoshio-Machi, Iizuka-City, Fukuoka 820-8505, Japan
[c] Pneumothorax Center, Nissan Tamagawa Hospital, 4-8-1 Seta, Setagaya-Ku, Tokyo 158-0095, Japan
[d] Fukuoka Clinic, 7-18-11 Umeda, Adachi-Ku, Tokyo 123-0851, Japan
[e] The Study Group of Pneumothorax and Cystic Lung Diseases, 4-8-1 Seta, Setagaya-Ku, Tokyo 158-0095, Japan

ARTICLE INFO

Article history:
Received 21 March 2012
Received in revised form 20 May 2012
Accepted 23 May 2012

Keywords:
Computed tomography
Lymphangioleiomyomatosis
Pulmonary function
Small pulmonary vessels

ABSTRACT

Backgrounds: Lymphangioleiomyomatosis (LAM) is a destructive lung disease that share clinical, physiologic, and radiologic features with chronic obstructive pulmonary disease (COPD). This study aims to identify those features that are unique to LAM by using quantitative CT analysis.
Methods: We measured total cross-sectional areas of small pulmonary vessels (CSA) less than 5 mm^2 and 5–10 mm^2 and calculated percentages of those lung areas (%CSA), respectively, in 50 LAM and 42 COPD patients. The extent of cystic destruction (LAA%) and mean parenchymal CT value were also calculated and correlated with pulmonary function.
Results: The diffusing capacity for carbon monoxide/alveolar volume (DL_{CO}/VA %predicted) was similar for both groups (LAM, 44.4 ± 19.8% vs. COPD, 45.7 ± 16.0%, $p = 0.763$), but less tissue damage occurred in LAM than COPD (LAA% 21.7 ± 16.3% vs. 29.3 ± 17.0; $p < 0.05$). Pulmonary function correlated negatively with LAA% ($p < 0.001$) in both groups, yet the correlation with %CSA was significant only in COPD ($p < 0.001$). When the same analysis was conducted in two groups with equal levels of LAA% and DL_{CO}/VA %predicted, %CSA and mean parenchymal CT value were still greater for LAM than COPD ($p < 0.05$).
Conclusions: Quantitative CT analysis revealing a correlation between cystic destruction and CSA in COPD but not LAM indicates that this approach successfully reflects different mechanisms governing the two pathologic courses. Such determinations of small pulmonary vessel density may serve to differentiate LAM from COPD even in patients with severe lung destruction.

1. Introduction

Lymphangioleiomyomatosis (LAM) is a rare cystic lung disease that is found primarily in women of childbearing age and is characterized by the proliferation of abnormal smooth muscle-like cells (LAM cells). The proliferation of LAM cells results in the destruction of lung tissue and associated lymphangiogenesis [1]. The cardinal physiologic and clinical consequences are impaired diffusing capacity and dyspnea on exertion. The most important disease to be differentiated from LAM is chronic obstructive pulmonary disease (COPD), because LAM and COPD share clinical, physiologic and radiologic features: dyspnea on exertion, airflow limitation, impaired diffusion, and lung destruction [2]. However, LAM usually progresses to respiratory insufficiency and afflicts patients younger than those with COPD. Additionally, the prognosis and management of these diseases are quite different. In patients with LAM, the immunosuppressive drug, sirolimus, has recently been found effective for stabilizing lung function [3,4].

Computed tomography (CT) is useful for differentiating between typical cases of LAM and COPD. Characteristics of the pulmonary cyst and low attenuation area (LAA), respectively, for LAM and COPD, provide a diagnostic clue [5,6]. In this context, high resolution CT image (HRCT) is better than conventional imaging. However, in patients with severe parenchymal destruction, simple visual assessment of CT images does not ensure the precise identification of LAM as distinct from COPD. For example, quantitative analysis of CT images can provide a correlation between low LAA and pulmonary function or symptoms in both LAM and COPD [7,8]. Yet, attention only to LAA on CT images, even with quantitative analysis, is insufficient for confident differentiation

* Corresponding author at: Department of Internal Medicine, Division of Respiratory Medicine, Juntendo University Graduate School of Medicine, 2-1-1 Hongo, Bunkyo-Ku, Tokyo 113-8421, Japan. Tel.: +81 35802 1063; fax: +81 35802 1617.
E-mail address: kando@juntendo.ac.jp (K. Ando).

0720-048X/$ – see front matter © 2012 Elsevier Ireland Ltd. All rights reserved.
http://dx.doi.org/10.1016/j.ejrad.2012.05.033

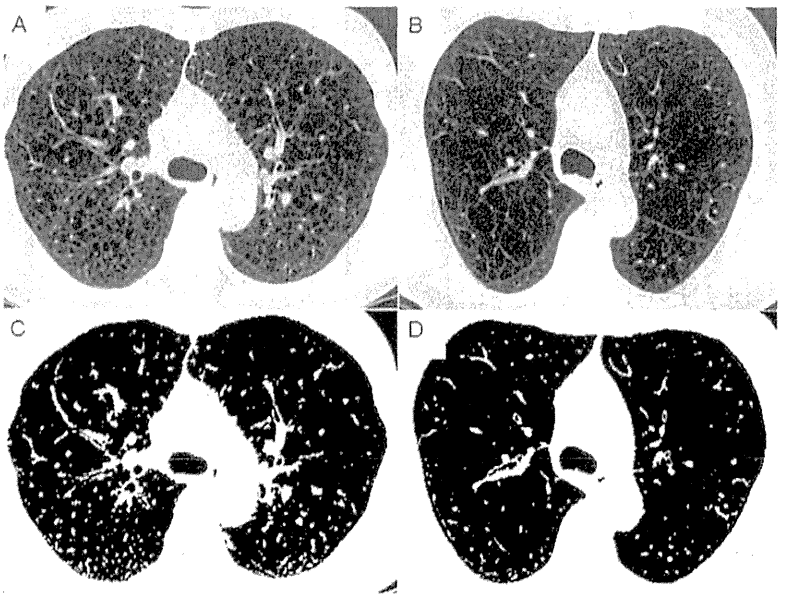

Fig. 1. Illustration of the procedure for measuring CSA on CT images in LAM (A and C) and COPD (B and D). The original images on which CSA is quantifiable appear in A (LAM) and B (COPD). First, a binary image was made from the original image using ImageJ software to measure CSA (C and D). Then, vessels that ran at an oblique angle to the axial plane were excluded using the "Circularity" function with a range from 0.9 to 1.0. The remaining white fields are CSA, which was measured by setting vessel size parameters within 0–5 mm^2 (CSA < 5) and 5–10 mm^2 (CSA 5–10). %CSA < 5 and %CSA 5–10 were determined as the percentage of each CSA per total lung area (C, 1.00% and 0.10%; D, 0.78% and 0.09%).

of LAM from COPD. Matsuoka et al. recently reported that a total cross-sectional area of small pulmonary vessels (CSA) on CT images could facilitate the assessment of COPD [9,10]. They revealed that the decrease in CSA strongly correlated with the extent of emphysema. Accordingly, we postulate that quantitative assessment of small pulmonary vessels can successfully differentiate LAM from COPD, since their underlying pathobiological mechanisms for parenchymal destruction are likely to differ. Therefore, we conducted quantitative CT analysis of CSA in patients with LAM and analyzed the correlation between CSA and pulmonary function. An identical analysis in patients with COPD followed to confirm if our analysis would duplicate the results for COPD reported by Matsuoka et al. Once we assured the reproducibility of our method, we compared the results of CSA analysis from patients with LAM and COPD to determine its success in differentiating them.

2. Methods

2.1. Study population

This retrospective and observational study was approved by the ethics committee of our institution (JH-21–134). We surveyed all patients who were diagnosed as having either LAM or COPD in the Department of Respiratory Medicine at Juntendo University Hospital from April 2006 to March 2008. After screening, we identified 50 patients with LAM and 42 with COPD, all of whom had undergone both a pulmonary function test and thin-section chest CT within the same 3-month period. We excluded patients who had obvious abnormal lung parenchymal lesions other than emphysema or cystic destruction: for example, pneumothorax, pleural effusion, pulmonary lymph edema or image noises that potentially interfered with image analysis. The diagnosis of LAM was established by histopathological examination ($n = 46$), or by clinical findings including the pulmonary function tests and characteristic appearance of chest HRCT ($n = 4$). The diagnosis of COPD was established based on the spirometric criteria of the GOLD guideline [11].

2.2. Analyses of thin-section CT images

Sequential CT scans were obtained using the 64-detector-row CT scanner (Aquilion-64; Toshiba Medical, Tokyo, Japan) with a 2-mm slice thickness, scanning parameters of 120 kVp, 150 mAs and a field of view of 32 cm. Three CT slices were selected for the measurement of CSA and LAA indicating cysts for LAM or emphysema for COPD, respectively. These were one above the upper margin of the aortic arch, 1 cm below the carina, and 1 cm above the right diaphragm. The CT images were analyzed using ImageJ software (a public domain Java image processing program available at http://rsb.info.nih.gov/ij/). LAA and total parenchymal lung area were defined as the area where the CT value was less than −960 HU and the one between −200 and −960 HU, respectively, and then LAA % was determined as the percentage of LAA per total lung area [8,12].

CSA was determined as reported by Matsuoka et al. [9,10]. As described and defined, we analyzed CSA at the subsegmental and sub-subsegmental levels separately: CSA less than 5 mm^2 (CSA < 5) was defined as the pulmonary vessels at the sub-subsegmental level and CSA with 5–10 mm^2 (CSA 5–10) as those at the subsegmental level [9,10]. Each step of the measurements presented in Fig. 1 was performed as follows. First, we segmented the lung field using a threshold technique with all pixels between −500 and −1024 HU and then made binary images, which were set up to window center of −720 HU, width of 1, and 8 bit of imaging type. Next we converted the binary images into segmented images using the "Make Binary" function. Vessels that ran at an oblique angle to the axial plane were excluded using the "Circularity" function with the range from 0.9 to 1.0 where "Circularity" measures the roundness of an object and was calculated as follows: circularity = 4π (area/m^2), and a value near 1.0 indicates that the object of concern is nearly circular. In this way, only those vessels whose long axis was orthogonal to the scanning plane were included in the CSA measurements. Finally, the percentages of CSA < 5 (%CSA < 5) and CSA 5–10 (%CSA 5–10) per parenchymal lung area that was defined as the area between −500 and −960 HU were determined on each

Table 1
Patients' characteristics and quantitative CT in LAM and COPD.

	LAM ($n=50$)	COPD ($n=42$)	p value
Age	36.8 ± 8.4	67.2 ± 8.3	<0.001
Male/Female	0/50	40/2	<0.001
Spirometry			
VC %pred (%)	94.1 ± 17.3	92.1 ± 16.0	0.621
FVC %pred (%)	89.7 ± 19.6	80.2 ± 17.8	<0.05
FEV_1 (L)	1.99 ± 0.66	1.41 ± 0.60	<0.001
FEV_1/FVC (%)	70.1 ± 18.6	48.6 ± 12.4	<0.001
FEV_1 %pred (%)	77.1 ± 25.0	53.8 ± 20.7	<0.001
DL_{CO}/VA %pred (%)	44.4 ± 19.8	45.7 ± 16.0	0.763
CT analysis			
LAA% (%)	21.7 ± 16.3	29.3 ± 17.0	<0.05
%CSA < 5 (%)	0.90 ± 0.33	0.72 ± 0.19	<0.01
%CSA 5–10 (%)	0.11 ± 0.05	0.09 ± 0.04	<0.05
CT value (HU)	−829.92 ± 28.01	−859.02 ± 27.94	<0.001

All data are presented as means ± SD.
CT value (HU) indicates the mean parenchymal CT value expressed with Hounsfield units.
Abbreviations used are: CSA, total cross sectional area of small pulmonary vessels; %CSA < 5 and %CSA 5–10, the percentages of CSA less than 5 mm^2 and CSA with 5–10 mm^2 per parenchymal lung area, respectively; DL_{CO}/VA, carbon monoxide diffusing capacity per alveolar gas volume; FEV_1, forced expiratory volume in one second; FVC, forced vital capacity; LAA%, the percentage of low attenuation area per total lung area; %pred, a percentage of the predicted values; and VC, vital capacity.

slice, and the means for %CSA < 5 and %CSA 5–10 of three selected CT images were obtained.

2.3. Pulmonary function tests

Pulmonary function tests were performed according to American Thoracic Society standards by using an Autospirometer System 9 or Autospirometer System 21 (Minato Medical Science, Osaka, Japan). Diffusing capacity for carbon monoxide (DL_{CO}) was measured using the single-breath technique and expressed as DL_{CO} per unit of alveolar volume (VA). Vital capacity (VC), forced vital capacity (FVC), forced expiratory volume in 1 s (FEV_1), and DL_{CO}/VA measurements for each patient were expressed as a percentage of the predicted values (VC %predicted, FVC %predicted, FEV_1%predicted and DL_{CO}/VA %predicted). The reference values obtained from the Japanese population were utilized to calculate the %predicted values [13].

2.4. Statistical analyses

To compare the patients' characteristics between those with LAM or COPD, we used χ^2 test or Mann–Whitney test where applicable and analyzed them with SPSS Version 19. Correlations of %CSA with LAA% and pulmonary function were evaluated by Spearman's rank correlation analysis. Data were expressed as means ± standard deviation. For all statistical analyses, a p value less than 0.05 was considered significant. Akaike's information criterion (AIC), which is a statistical value known to provide a superior fit, was applied to obtain the most appropriate cut-off level for FEV_1%predicted and DL_{CO}/VA %predicted [14]. A smaller AIC value indicated a more reliable model for predicting a discrimination of LAM from COPD.

3. Results

3.1. Patients' characteristics

The characteristics of patients' LAM ($n=50$) and COPD ($n=42$) are shown in Table 1. All LAM patients were female, and their mean age was younger than those in the mixed-gender COPD group (36.8 vs. 67.2 years, respectively, $p<0.001$). VC %predicted and DL_{CO}/VA %predicted were not statistically different in the two groups; however, airflow was more severely limited in COPD than LAM, as indicated by significantly diminished FVC %predicted, FEV_1/FVC, FEV_1%predicted in COPD. We then examined the relationship between FEV_1%predicted and DL_{CO}/VA %predicted in LAM and COPD (Fig. 2). All LAM and COPD patients showed a negative correlation between FEV_1%predicted and DL_{CO}/VA %predicted, but the correlation coefficient was much greater in the LAM group ($r=0.833$, $p<0.001$ vs. $r=0.288$, $p<0.001$, respectively). This difference might have represented patients with LAM who had a diminished DL_{CO}/VA %predicted without an airflow limitation (Fig. 2).

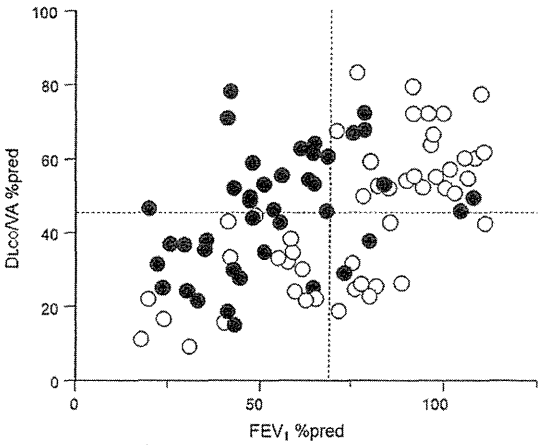

Fig. 2. Relationship between FEV_1%predicted and DL_{CO}/VA %predicted in LAM (○) and COPD (•). LAM showed a stronger negative correlation between FEV_1%predicted and DL_{CO}/VA %predicted than COPD ($r=0.833$, $p<0.001$ vs. $r=0.288$, $p<0.001$, respectively). Broken lines indicate FEV_1 70% predicted and DL_{CO}/VA 45% predicted as determined by AIC analysis (see Section 2) to identify the most appropriate cut-off level for the discrimination of LAM from COPD (AIC = −29.30). Note that LAM patients were the most likely to have both $FEV_1 \geq 70\%$ predicted and $DL_{CO}/VA \geq 45\%$ predicted, although that tendency did not reach the level of statistical significance ($p=0.054$).

To determine the most appropriate cut-off level of FEV_1%predicted and DL_{CO}/VA %predicted, the AIC was calculated. As a result, the smallest AIC value for the most appropriate cut-off levels of FEV_1%predicted and DL_{CO}/VA %predicted were 70% and 45%, respectively (AIC = −29.30), and this revealed that patients with FEV_1%predicted ≥ 70% and DL_{CO}/VA %predicted ≥ 45% are the most likely to have LAM ($p=0.056$).

3.2. Results of quantitative CT

In accord with greater limitation of airflow in COPD than LAM, quantitative CT revealed that lung destruction represented by LAA% was more severe in COPD (COPD, 29.3 ± 17.0% vs. LAM, 21.7 ± 16.3%, $p<0.05$) (Table 1). Although both groups had the same degree of impairment in DL_{CO}/VA %predicted, values for %CSA < 5, %CSA 5–10, and mean parenchymal CT differed significantly. Since the patient's age obviously differed between LAM and COPD, we also examined the correlation between age and %CSA < 5 or %CSA 5–10 by using partial correlation analysis, but found no statistical significance ($r=-0.149$, $p=0.163$ for %CSA < 5 and $r=0.065$, $p=0.545$ for %CSA 5–10). That is, regardless of age, LAM patients had higher densities of pulmonary small vessels as well as parenchymal areas than COPD patients when the groups with the same degree of impaired diffusing capacity were compared.

We next examined the relationship between LAA% and %CSA in LAM and COPD (Fig. 3). As reported by Matsuoka et al. [9], both %CSA < 5 and %CSA 5–10 showed weak but statistically significant

Table 2
Correlation betweenCT measurement and pulmonary function.

	LAM		COPD	
	r	*p* value	*r*	*p* value
LAA%				
VC %pred*	0.020	0.890	0.059	0.709
FVC %pred	−0.134	0.353	−0.195	0.217
FEV_1/FVC	−0.780	<0.001	−0.713	<0.001
FEV_1%pred	−0.623	<0.001	−0.570	<0.001
DL_{CO}/VA %pred	−0.808	<0.001	−0.700	<0.001
%CSA < 5				
LAA%	−0.211	0.141	−0.686	<0.001
VC %pred	−0.002	0.987	0.084	0.595
FVC %pred	0.015	0.916	0.298	0.055
FEV_1/FVC	−0.002	0.989	0.608	<0.001
FEV_1%pred	−0.109	0.449	0.509	<0.01
DL_{CO}/VA %pred	−0.152	0.296	0.356	<0.05
%CSA 5–10				
LAA%	−0.039	0.786	−0.467	<0.01
VC %pred	−0.096	0.508	0.021	0.895
FVC %pred	−0.086	0.554	0.180	0.254
FEV_1/FVC	0.245	0.086	0.358	<0.05
FEV_1%pred	0.172	0.231	0.349	<0.05
DL_{CO}/VA %pred	0.257	0.075	0.291	0.065

Abbreviations used are as same as those in Table 1.

negative correlations with LAA% in COPD. In contrast, LAM showed no correlation between %CSA and LAA%.

3.3. Correlation between quantitative CT and pulmonary function

The correlation between CT measurement and pulmonary function is shown in Table 2. In both LAM and COPD, LAA% had statistically significant negative correlation with FEV_1/FVC ($r = -0.780$ and -0.713, respectively), FEV_1%predicted ($r = -0.623$ and -0.570), and DL_{CO}/VA %predicted ($r = -0.808$ and -0.700). Meanwhile, values from patients with COPD had statistically significant correlations between %CSA and the indices of airflow limitation such as FEV_1/FVC ($r = 0.608$ for %CSA < 5 and 0.358 for %CSA 5–10, respectively) and FEV_1%predicted ($r = 0.509$ and 0.349), and between DL_{CO}/VA %predicted and %CSA < 5 alone ($r = 0.356$).

Table 3
Comparison of %CSA < 5 and %CSA 5–10 between LAM and COPD patients who had LAA% ≥ 5%.

	LAM ($n = 42$)	COPD ($n = 41$)	*p* value
LAA% (%)	25.4 ± 15.1	29.9 ± 16.7	0.222
%CSA < 5 (%)	0.85 ± 0.27	0.71 ± 0.19	<0.05
%CSA 5–10 (%)	0.12 ± 0.05	0.09 ± 0.04	<0.05
CT value (HU)	−833.19 ± 26.84	−859.93 ± 25.81	<0.001
DL_{CO}/VA %pred (%)	40.75 ± 18.59	45.09 ± 15.63	0.337

All data are presented as means ± SD.
Abbreviations used are as same as those in Tables 1 and 2.

These results regarding COPD in our study were similar to those reported by Matsuoka et al. [9]. In contrast, no significant correlation was evident in LAM between small pulmonary vessels (%CSA < 5 and %CSA 5–10) and pulmonary function.

3.4. Comparison of LAM and COPD patients with equivalent lung destruction (LAA%)

In our study, LAM and COPD groups had same degree of DL_{CO}/VA %predicted, but differed notably in the extent of lung destruction represented by LAA% (Table 1). Accordingly, we examined the densities of small pulmonary vessels (%CSA) and lung parenchyma (mean parenchymal CT value) in individuals from both disease categories with same degree of lung destruction (LAA% ≥ 5%): 42 LAM patients and 41 COPD patients were selected for this analysis (Table 3). In a comparison of the two groups, LAA% and DL_{CO}/VA %predicted were similar. However, %CSA < 5, %CSA 5–10 and the mean parenchymal CT value were significantly higher in LAM than COPD. We performed the same analysis in the patients with LAA% ≥ 10% ($n = 38$ for LAM and 37 for COPD), those with LAA% ≥ 20% ($n = 22$ and 26, respectively), and again, LAM patients had higher small pulmonary vessel densities and parenchymal densities than COPD patients when both groups had the same extent of LAA%.

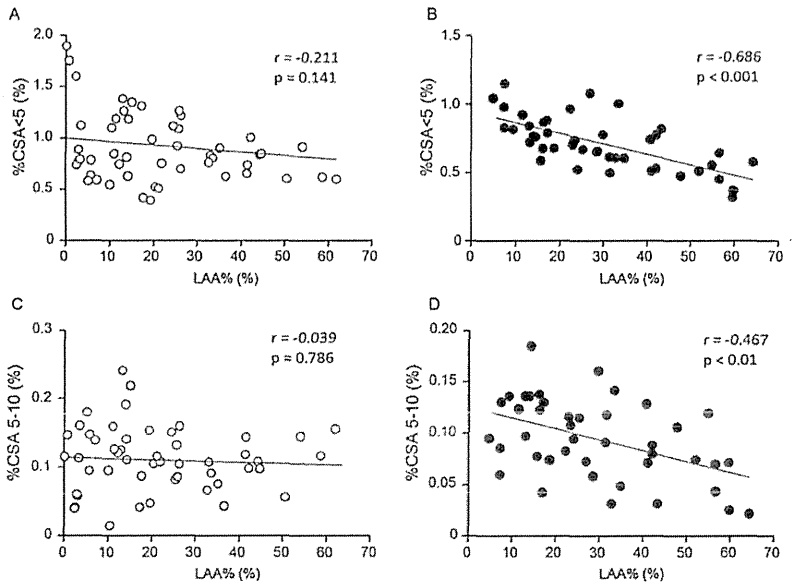

Fig. 3. Relationships between %CSA < 5 or %CSA 5–10 and LAA% in LAM (○) and COPD (•). The relationships between %CSA < 5 (A and B) or %CSA 5–10 (C and D) and LAA% are shown in each panel. A statistically significant negative correlation between %CSA < 5 (B) or %CSA 5–10 (D) and LAA% is demonstrated in COPD, but not in LAM (A and D).

4. Discussion

In this quantitative CT study, we have demonstrated for the first time important physiologic and radiologic features of patients with LAM contrasted with those who have COPD. That is, the extent of small pulmonary vessel impairment is not likely to have an intimate relationship with the extent of lung destruction and abnormalities of pulmonary function, including diffusing capacity for carbon monoxide, in LAM, although it does in COPD (1) the %CSA was higher in LAM than in COPD, although both groups showed the same degree of impairment in DL_{CO}/VA %predicted, (2) %CSA was still higher in LAM even when individuals with LAM and COPD who had the same extent of LAA% were selected, (3) although LAA% showed a significantly negative correlation with lung function in both LAM and COPD, the %CSA showed no correlation with LAA% or pulmonary function in LAM but did correlate with both values in COPD. Matsuoka et al. first reported a negative correlation between %CSA and LAA% in COPD by quantitative analysis of CT images [9]. The mechanisms for this negative correlation was attributed to the decrease of small pulmonary vessels related to parenchymal destruction as well as passive vascular compression due to the progression of emphysema, hypoxic vasoconstriction, and endothelial dysfunction [9,15,16]. The results of our study suggest that cystic lung destruction does not necessarily accompany a concomitant loss of pulmonary vasculature in LAM. This may be supported by the findings that LAM lesions are scattered in an intervening normal lung parenchyma [1,17] and that LAM involves higher mean parenchymal CT values than COPD.

Impairment of DL_{CO} is the abnormality of pulmonary function most frequently seen in LAM patients [18]. Furthermore, a diminished DL_{CO} without airflow limitation seems to be the sole abnormality found in an early stage of LAM [19]. In our study population, the LAM group showed milder airflow limitation and lung destruction (LAA%) than those found in COPD, yet both groups had the same degree of impairment in DL_{CO}/VA %predicted (Table 1). In LAM, the lungs are pathologically characterized by the cystic destruction that is distributed diffusely and distinctly with an intervening normal lung parenchyma, due to the proliferation of LAM cells and the abundant lymphatic vessels caused by LAM-associated lymphangiogenesis [1,2,19,20]. Based on these pathologic characteristics of lungs, we speculate that LAM patients have higher values in both %CSA and parenchymal CT than COPD patients do for the following reasons (1) lung tissue, aside from cystic destruction, is well-preserved in LAM in contrast to COPD, (2) proliferation of LAM cells and LAM-associated lymphangiogenesis with increased intrapulmonary lymphatic flow may be the result, and (3) these LAM-related pathophysiologic abnormalities are more directed toward impaired diffusion than cystic destruction in LAM.

Our study indicates that the determination of CSA by quantitative CT analysis provides the opportunity to differentiate LAM from COPD. LAM is found primarily in women of childbearing age and is sometimes related to tuberous sclerosis complex. Therefore, such factors as age and gender usually contribute to an accurate diagnosis of LAM. Furthermore, the characteristic CT appearance of multiple thin-walled cysts which are usually round and distributed evenly throughout the lungs with normal lung parenchyma has a bearing on the diagnosis of mild to moderate LAM [5,6]. However, in patients with advanced LAM and severe parenchymal destruction, simple visual assessment of CT images would not ensure the precise differentiation between LAM and COPD. Establishing a definitive diagnosis on pathological grounds is important, but invasive examination such as lung biopsy cannot be performed in the victims of advanced LAM whose parenchyma is severely damaged. Our study suggests that quantitative assessment of small pulmonary vessel density on CT images may provide alternative and additive information for diagnosing patients with advanced LAM.

Our study has some limitations. First, the number of the patients included in this retrospective analysis was relatively small, so the results obtained may be biased. However, our results for COPD were similar to those of previous studies used as a precedent [9]. Additionally, considering the rarity of LAM, our analysis of 50 LAM patients places it in the context of quite a sizeable population that warrants attention. Second, although our analysis elucidated the possible pathophysiologic features of LAM that differentiates it from COPD, we did not obtain pathologic confirmation. Accordingly, some of the objects considered as the small pulmonary vessels on CT images may have been the abundant lymphatic vessels and small LAM nodules, to be confirmed by further evaluation.

In conclusion, quantitative CT analysis revealed that neither LAA% nor DL_{CO}/VA %predicted showed a significant correlation with %CSA in LAM as compared with COPD. However, a quantitative determination of CSA allowed us to clearly differentiate LAM from COPD even in a LAM patient with severe lung destruction. Our results support clinical findings that some LAM patients, even at an early stage of the disease, show an impaired diffusing capacity that appears to be out of proportion to the degree of airflow limitation and attribute this impairment to unique LAM-associated pathophysiologic mechanisms, rather than simple destruction of lung parenchyma.

Acknowledgments

We thank Phyllis Minick for excellent assistance in the review of English. This study was supported by a grant to the Respiratory Research Group from the Ministry of Health, Labour and Welfare, Japan; in part by the High Technology Research Center Grant from the Ministry of Education, Culture, Sports, Science, and Technology, Japan; and in part by the Institute for Environmental and Gender-Specific Medicine, Juntendo University, Graduate School of Medicine.

References

[1] Corrin B, Liebow AA, Friedman PJ. Pulmonary lymphangiomyomatosis. A review. The American Journal of Pathology 1975;79(2):348–82.
[2] McCormack FX. Lymphangioleiomyomatosis: a clinical update. Chest 2008;133(343):507–16.
[3] Bissler JJ, McCormack FX, Young LR, et al. Sirolimus for angiomyolipoma in tuberous sclerosis complex or lymphangioleiomyomatos. The New England Journal of Medicine 2008;358(2):140–51.
[4] McCormack FX, Inoue Y, Moss J, et al. Efficacy and safety of sirolimus in lymphangioleiomyomatosis. The New England Journal of Medicine 2011;364(17):1595–606.
[5] Lenoir S, Grenier P, Brauner MW, et al. Pulmonary lymphangiomyomatosis and tuberous sclerosis: comparison of radiographic and thin-section CT findings. Radiology 1990;175(2):329–34.
[6] Johnson SR, Cordier JF, Lazor R, et al. European respiratory society guidelines for the diagnosis and management of lymphangioleiomyomatosis. European Respiratory Journal 2010;35(1):14–26.
[7] Tobino K, Hirai T, Johkoh T, et al. Differentiation between Birt-Hogg-Dubé syndrome and lymphangioleiomyomatosis: quantitative analysis of pulmonary cysts on computed tomography of the chest in 66 females. European Journal of Radiology 2011;5 [Epub ahead of print].
[8] Mishima M, Hirai T, Itoh H, et al. Complexity of terminal airspace geometry assessed by lung computed tomography in normal subjects and patients with chronic obstructive pulmonary disease. Proceedings of the National Academy of Sciences of the United States of America 1999;96(16):8829–34.
[9] Matsuoka S, Washko GR, Dransfield MT, et al. Quantitative CT measurement of cross-sectional area of small pulmonary vessel in COPD: correlations with emphysema and airflow limitation. Academic Radiology 2010;17(1):93–9.
[10] Matsuoka S, Washko GR, Yamashiro T, et al. Pulmonary hypertension and computed tomography measurement of small pulmonary vessels in severe emphysema. American Journal of Respiratory and Critical Care Medicine 2010;181(3):218–25.
[11] Global Initiative for Chronic Obstructive Lung Disease (GOLD). Global strategy for the diagnosis, management, and prevention of chronic obstructive pulmonary disease (updated 2011). Bethesda, MD: National Heart, Lung and Blood Institute/World Health Organization; 2011.
[12] Sakai N, Mishima M, Nishimura K, Itoh H, Kuno K. An automated method to assess the distribution of low attenuation areas on chest CT scans in chronic pulmonary emphysema patients. Chest 1994;106(5):1319–25.

[13] Sharp DS. Reference values for lung function in the Japanese: recording of normal lung function from 11 institutes in Japan. Japan Journal of Thoracic Diseases 1993;31:421–7.
[14] Akaike H. A new look at statistical model identification. IEEE Transactions on Automatic Control 1974;19:716–23.
[15] Santos S, Peinado VI, Ramirez J, et al. Enhanced expression of vascular endothelial growth factor in pulmonary arteries of smokers and patients with moderate chronic obstructive pulmonary disease. American Journal of Respiratory and Critical Care Medicine 2003;167(9):1250–6.
[16] Barr RG, Mesia-Vela S, Austin JH, et al. Impaired flow-mediated dilation is associated with low pulmonary function and emphysema in ex-smokers: the emphysema and cancer action project (EMCAP) study. American Journal of Respiratory and Critical Care Medicine 2007;176(12): 1200–7.
[17] Matsui K, Beasley MB, Nelson WK, et al. Prognostic significance of pulmonary lymphangioleiomyomatosis histologic score. American Journal of Surgical Pathology 2001;25(4):479–84.
[18] Kitaichi M, Nishimura K, Itoh H, Izumi T. Pulmonary lymphangioleiomyomatosis: a report of 46 patients including a clinicopathologic study of prognostic factors. American Journal of Respiratory and Critical Care Medicine 1995;151:527–33.
[19] Seyama K, Kira S, Takahashi H, et al. Longitudinal follow-up study of 11 patients with pulmonary lymphangioleiomyomatosis: diverse clinical courses of LAM allow some patients to be treated without anti-hormone therapy. Respirology 2001;6(4):331–40.
[20] Kumasaka T, Seyama K, Mitani K, et al. Lymphangiogenesis-mediated shedding of LAM cell clusters as a mechanism for dissemination in lymphangioleiomyomatosis. American Journal of Surgical Pathology 2005;29(10):1356–66.